

Angular rigidity in tetrahedral network glasses with changing compositionM. Bauchy,¹ M. Micoulaut,¹ M. Celino,² S. Le Roux,³ M. Boero,³ and C. Massobrio³¹*Laboratoire de Physique Théorique de la Matière Condensée, Université Pierre et Marie Curie, Boite 121, 4, Place Jussieu, F-75252 Paris Cedex 05, France*²*ENEA, Italian National Agency for New Technologies, Energy and Sustainable Economic Development, C. R. Casaccia, Via Anguillarese 301, 00123 Rome, Italy*³*Institut de Physique et de Chimie des Matériaux de Strasbourg, 23 rue du Loess, BP43, F-67034 Strasbourg Cedex 2, France*
(Received 6 June 2011; published 1 August 2011)

A set of oxide and chalcogenide tetrahedral glasses is investigated using molecular dynamics simulations. We show that the changes in the Ge composition affect mostly bending around germanium in binary Ge-Se systems, leaving Se-centered bending almost unchanged. In contrast, the corresponding Se twisting (quantified by the dihedral angle) depends on the Ge composition and is reduced when the system becomes rigid. It is also shown that angles involving the fourth neighbor around Ge is found to change when the system enters the stressed rigid phase. The same analysis reveals that unlike stoichiometric selenides such as GeSe₂ and SiSe₂, germania and silica display large standard deviations in the bond angle distributions. Within bond-bending constraints theory, this pattern can be interpreted as a manifestation of *broken* (i.e., ineffective) oxygen bond-bending constraints, whereas the silicon and germanium bending in oxides is found to be similar to the one found in flexible and intermediate Ge-Se systems. Our results establish the atomic-scale foundations of the phenomenological rigidity theory, thereby profoundly extending its significance and impact on the structural description of network glasses.

DOI: [10.1103/PhysRevB.84.054201](https://doi.org/10.1103/PhysRevB.84.054201)

PACS number(s): 61.43.Fs

I. INTRODUCTION

The large variety (Ref. 1) of physicochemical behaviors inherent in tetrahedral network glasses [in particular, those involving Group IV ($A = \text{Si, Ge}$) oxides ($X = \text{O}$) or chalcogenides ($X = \text{S, Se, Te}$)] is deeply related to the underlying network topology [i.e., the nature of the connections (edge or corner sharing) among the basic tetrahedral structural units.^{2,3}] In the search for a unifying approach, it is tempting to follow rigidity theory, which describes the interplay between network properties and connectivity by considering covalent networks in very much the same fashion as mechanical trusses.^{4,5} This is achieved via enumeration of mechanical rigid constraints n_c arising from relevant atomic interactions, $r/2$ bond stretching (BS, radial) and $(2r - 3)$ bond bending (BB, angular) for an atom with coordination r .

According to rigidity theory, the glass-forming ability and the compositional trends in physical and chemical properties are determined by comparing n_c with the number of atomic degrees of freedom (i.e., 3 in 3 dimensions). A central result of rigidity theory is the identification of a rigidity transition at the network mean coordination number $\bar{r} = 2.4$, separating underconstrained networks having low-frequency (floppy) deformation modes ($n_c < 3$) from overconstrained ones ($n_c > 3$) (Refs. 4 and 5). The optimum glass compositions are those in which n_c equals exactly the number of degrees of freedom, leading to an isostatic glass. A number of studies on the determination of bulk glass-forming regions in binary and ternary network glasses have shown that samples could be rather easily produced close to compositional joins satisfying $n_c \simeq 3$. In Ge-Se systems, slow cooling allows only glass formation at network connectivities that are somewhat lower than the critical coordination number $\bar{r} = \bar{r}_c = 2.4$. An increase of the cooling rate (from air quench to water quench) increases the glass-forming region⁶ up to $\bar{r} = 2.67$

where stress-induced phase separation occurs.^{7,8} Similarly, in silicates the critical cooling rate⁹ to avoid crystallization is found to be minimum at compositions close to the optimal constrained compositions.^{10,11}

As mentioned above, the main input for the constraint enumeration in rigidity theory are the coordination numbers of the involved atoms and the relevant atomic interactions (BS, BB) which are effective as mechanical rigid constraints. Defining a simple link between n_c and such quantities (coordination numbers, interactions) is highly contentious. For instance, there has been an unsuccessful search for the effect of increasing stress on the local atomic structure. While numerical models have suggested that there is a link between the increase of rigidity and bond mismatch^{12,13} (i.e., a decreased accommodation to obtain the zero stress bond length), no obvious structural signatures of rigidity transitions have been found from neutron or high energy x-ray diffraction on the position of the width of e.g., the first sharp diffraction peak.^{14,15}

On a separate and also debated issue, for stoichiometric compositions like GeSe₂ or GeS₂, with Ge and Se (or S) forming, respectively, four-fold and two-fold units, one obtains 2 BS (respectively 1) and 5 BB constraints (respectively 1), leading on the overall to $n_c = 3.67$ (i.e., such glasses should be rigid and overconstrained). As a result, because of the higher stress piled in the network, these glasses are found at the very limit of the binary glass-forming region (in, e.g., Ge_xSe_{1-x}, Ref. 16). At a first glance, the corresponding oxides (GeO₂ and SiO₂) should be analogous to the stoichiometric GeSe₂ with a mean coordination number $\bar{r} = 2.67$, and $n_c = 3.67$. However, the legitimacy of such a simple picture is challenged by a certain number of experimental observations. One has first to remark that silica (SiO₂) and germania (GeO₂) are found to form rather easily glasses,¹⁷ in contrast with the corresponding

chalcogenides (e.g., GeSe₂, Ref. 18 and 19). Furthermore, oxides have a low frequency (floppy) contribution in the vibrational density of states, suggesting that these systems are flexible²⁰ or, at least, nearly optimally constrained²¹ (isostatic, $n_c = 3$). The latter result can be recovered in rigidity theory under the heuristic assumption that enhanced oxygen bond-angle values within a broad Si-O-Si distribution should lead to *broken* angular constraints²² reducing n_c from 3.67 to 3.0. This assumption is challenged by recent studies^{23,24} showing that the Si-O-Si angle is significantly narrower in SiO₂, at odds with previous work on the experimental determination of the silica bond angle distribution.²⁵

Here we propose a very general method^{26,27} which allows to compute such constraints without any prerequisite on coordination numbers or interactions. We rely on an atomic-scale approach (as molecular dynamics, MD) which is able to substantiate and enrich the general trends of rigidity theory via the explicit account of the corresponding local structure. This allows to bridge the gap between constraint counting algorithms based merely on coordination numbers (bound to fail in certain situations),²⁸ and the statistical mechanical behavior of relevant atomic-scale quantities (radial and angular distributions) on which counting algorithms are applied. A set of nine different chalcogenides and oxide glasses are investigated: five compositions in the Ge_xSe_{1-x} system, SiO₂, GeO₂, SiSe₂, and a densified GeSe₂ glass.

First, we find that in the binary Ge_xSe_{1-x} system with increasing Ge content, structural changes are mostly noticeable in the angular environment of the germanium atoms, leaving the Se centered angular excursions (quantified by σ_θ , the standard deviation of partial bond angle distributions) nearly unchanged when moving from a flexible to a stressed rigid phase. It appears that the amplitude of the angular excursion around Ge atoms is increased in the stressed rigid phase with an increased distortion of the tetrahedra. This result allows reconsidering the general accepted picture of a Ge-Se network made of flexible Se-chains and rigid GeSe_{4/2} tetrahedra.⁴ We analyze in a similar fashion a densified GeSe₂ glass, and find an important decrease of the edge-sharing fraction. The tetrahedral distortion is even more enhanced as compared to ambient GeSe₂, suggesting that pressure-induced stress also acts on the Ge angular motion. In addition, we provide insight into the nature of the chemical bonding in Ge_xSe_{1-x} via an analysis of the correlations between the atomic centers and the localized Wannier centers. This information is readily obtained from an analysis of the electronic structure of our systems.

We finally focus also on the stoichiometric AX₂ compositions (i.e., SiO₂, GeO₂, SiSe₂, and GeSe₂) and show that oxide systems contain tetrahedra which act as rigid units having a much smaller minimal angular excursion for the Group IV element than their chalcogenide counterparts. Specifically, we find that such excursions for oxygen in oxides are much larger than those for selenium in GeSe₂, suggesting that oxygen bending constraints are, in fact, *broken* (i.e., ineffective) in SiO₂ and GeO₂. This provides a microscopic rationale for the sensitivity to bond-bending around oxygen in oxide networks, consistent with experimental evidence.²²

Although we apply these methods to archetypal network glasses, the rationale developed here is novel and insightful

especially for the case of bond-bending constraints. Methods based on the atomic scale trajectories are prone to be applied also to glasses incorporating charge-compensating cations²⁹ or pressure-induced rigidity.²⁰

II. SIMULATION METHODOLOGY

Our analysis is based on molecular dynamics trajectories obtained at $T = 300$ K for a set of glassy systems encompassing GeO₂, SiO₂, SiSe₂, and Ge_xSe_{1-x} for five different compositions: $x = 0.10$ (GeSe₉ in the flexible phase), $x = 0.20$ (GeSe₄ at the rigidity transition³⁰), $x = 0.25$ (GeSe₃ in the Boolchand intermediate phase),^{16,18,19} $x = 0.33$ (GeSe₂), and $x = 0.40$ (Ge₂Se₃, both in the stressed rigid phase). Oxides at the experimental densities have been simulated according to Refs. 31 and 32 using a classical Born-Mayer force field. Due to the large difference of electronegativity between Si(Ge) and O, this choice ensures plausible qualitative modeling within classical molecular dynamics. In the case of SiSe₂ and Ge_xSe_{1-x} systems, we resort to first-principles molecular dynamics (FPMD) within a fully self-consistent framework that proved adequately to describe chemical bonding and its changes with concentration.³³ For some of the systems, temporal trajectories recorded previously³⁴ are substantially extended to attain optimal statistical accuracy (within a few percent at most). Otherwise, as in the case of GeSe₉ and GeSe₃, glassy structures are produced from the outset after cooling from the liquid state and appropriate structural relaxation. Overall, typical time trajectories for collection of the averages in the glassy state cover ~ 100 ps. Details on the FPMD methodology and the productions of glassy structure are extensively reported in Refs. 34–42. For all glassy structures, the atomic-scale picture is consistent with that obtained by using an alternative first-principles approach.^{43–47} The densified GeSe₂ system has been produced from the starting ambient GeSe₂ glass, with a gradual change in the system cell length, leading at the end to an increase in density of 15.5%, and a corresponding pressure of 3 GPa.

We are interested in determining the sensitivity of chemical bonding to the composition. To this purpose, an insight into the bonding localization properties can be achieved by the formalism of the Boys localized orbitals.⁴⁸ Since we use a supercell approach, the Boys localized orbitals are calculated as their periodic system generalization, namely the maximally localized Wannier functions^{49,50} (WF) and the weighted center of their charge distribution [i.e., the Wannier functions centers (WFC)]. An analysis in terms of localized orbitals were performed by computing the WFs and WFCs. Namely, WFs are obtained by a unitary transformation of the occupied Bloch orbitals. It should be recalled that, in principle, the WFs are not uniquely defined, due to the arbitrary phase factor of the Bloch orbitals. This indeterminacy has been resolved in Ref. 50 by requiring that the total spread of the Wannier functions

$$S = \sum_n (\langle r^2 \rangle_n - \langle \mathbf{r} \rangle_n^2), \quad (1)$$

be minimized in real space.

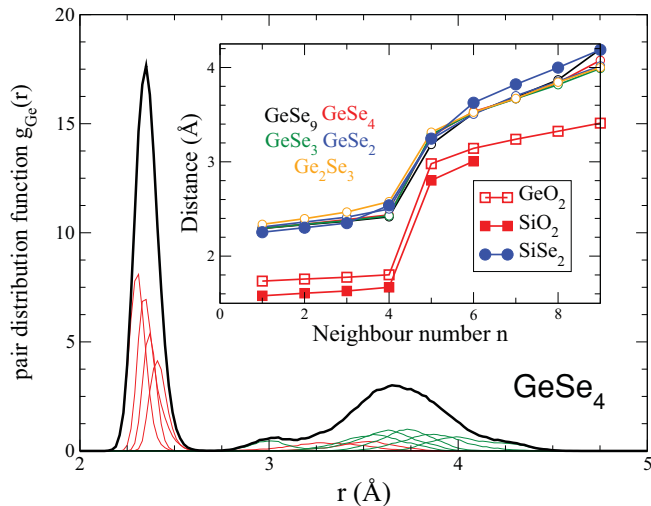


FIG. 1. (Color online) Neighbor distribution functions (NDF) (red: neighbors 1–4, green: neighbors 5–9) around a central Ge atom in glassy GeSe_4 . The sum of the nine distributions yields the pair distribution function at low distance (black curve). The insert shows corresponding neighbor (NDF) peak positions as a function of the neighbor number for SiSe_2 (filled circles), SiO_2 , GeO_2 (filled boxes), and $\text{Ge}_x\text{Se}_{1-x}$ (open circles).

III. RESULTS

A. Bond stretching

To obtain the number of bond-stretching interactions we have focused on neighbor distribution functions (NDFs). A set of NDFs can be defined by fixing the neighbor number n (first, second, etc), the sum of all NDFs yielding the standard pair distribution function $g_i(r)$ ($i = A, X$). Integration of $g_i(r)$ ($i = A, X$) up to the first minimum gives the coordination numbers r_X and r_A , and hence the corresponding number of bond-stretching constraints $r_i/2$ ($i = A, X$). Figure 1 shows such application to the GeSe_4 glass. Four NDFs (red curves) contribute to the first peak of $g_{\text{Ge}}(r)$, very well separated from the second shell of neighbors (green curves), and indicative of the presence of four neighbors around a Ge atom. The separation between the first and second shells of neighbors can be also characterized by plotting the NDF peak positions as a function of the neighbor number (inset of Fig. 1). One sees that there is a clear gap in the distance between $n = 4$ and $n = 5$ for all considered systems. Here one can furthermore remark that in $\text{Ge}_x\text{Se}_{1-x}$, there is almost no change in the neighborhood of Ge atoms. Thus, we find $r_X = 2$ and $r_A = 4$ leading to 1 and 2 bond-stretching constraints for the X and A atoms at any composition. When integrating the pair distribution function up to its first minimum, we find for GeO_2 $r_{\text{Ge}} = 4.01$ and $r_{\text{O}} = 1.97$, and for GeSe_2 , $r_{\text{Ge}} = 4.02$ and $r_{\text{Se}} = 1.96$, in agreement with experiments.^{3,51,52}

B. Bond bending

The bond-bending constraint counting is based on partial bond angle distributions (PBADs) $P(\theta_{ij})$ defined as follows: for each type of central atom 0, the N first neighbors i are selected and the $N(N-1)/2$ corresponding angles $i0j$ ($i = 1, \dots, N-1, j = 2, \dots, N$) computed (i.e., 102, 103,

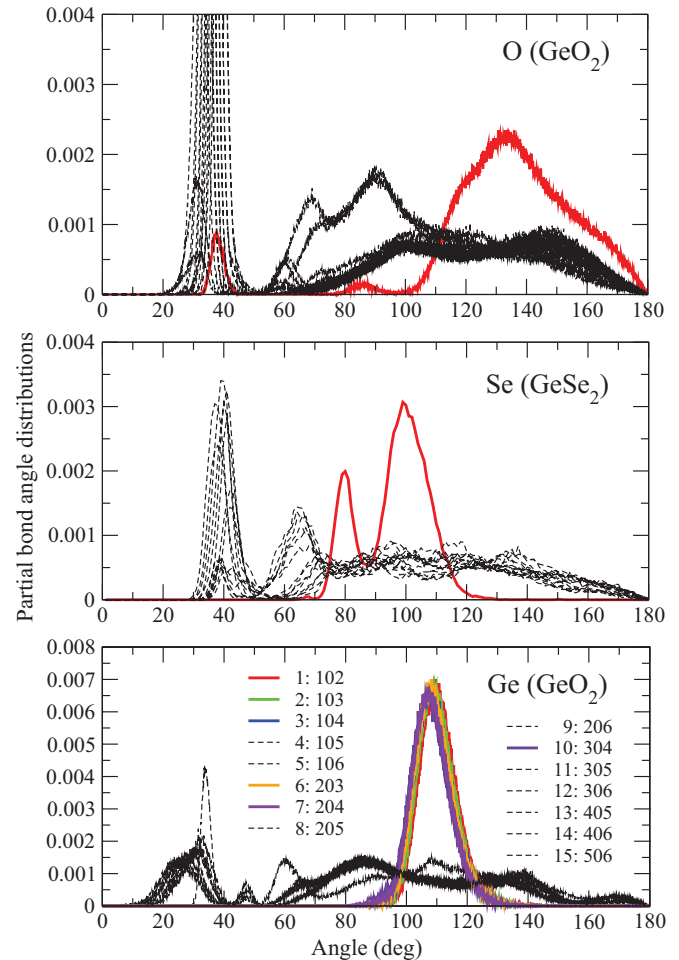


FIG. 2. (Color online) From top to bottom: oxygen, selenium, and germanium partial bond angle distributions (PBAD) in GeO_2 and GeSe_2 for an arbitrary $N = 6$. The colored curves correspond to PBADs having the lowest standard deviation(s) σ_θ . The sharp peaks at $\theta \simeq 40^\circ$ correspond to the hard-core repulsion. Labels defined in the bottom panel are used throughout the text.

203, etc.). The standard deviation $\sigma_{\theta_{ij}}$ [written as σ_θ or σ_i ($i = X, A$) in the following] of each distribution $P(\theta_{ij})$ gives a quantitative estimate of the angular excursion around a mean angular value, and provides a measure of the bond-bending strength.^{26,27} Small values for σ_θ correspond to an intact bond-bending constraint which maintains a rigid angle at a fixed value, whereas large σ_θ correspond to a bond-bending weakness giving rise to an ineffective or *broken* constraint.

The results of such an analysis are shown in Fig. 2 for GeO_2 and GeSe_2 . Broad distributions are found in most of the situations, together with a certain number of sharper distributions (colored) which will be identified as intact angular constraints. The oxygen PBAD 102 is found to be centered at 135° , close to the value obtained from experiments,⁵³ whereas the corresponding selenide distribution shows a bimodal distributions with peaks at 80° and 100° , indicative of edge- and corner-sharing tetrahedra,³⁸ respectively. This feature is absent in the oxides. For the Ge-centered PBAD in GeO_2 , one finds six nearly identical distributions at 109° , defining the tetrahedra. From all these different distributions, a second

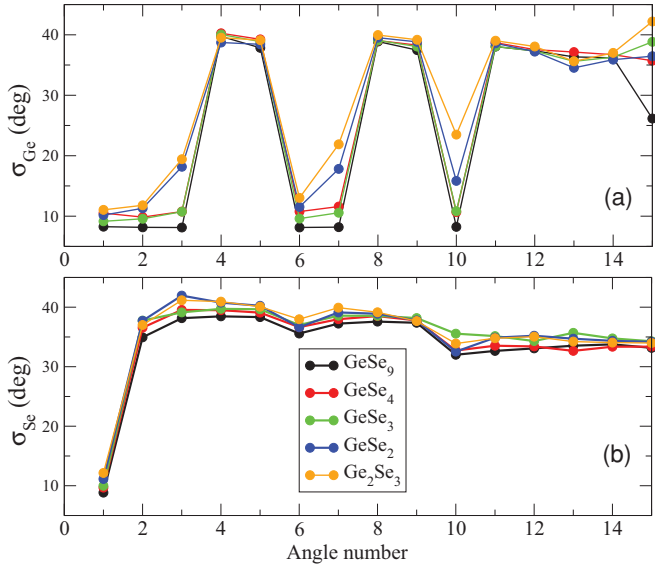


FIG. 3. (Color online) Standard deviation σ_{Ge} and σ_{Se} extracted from the partial bond angle distributions (PBAD) for five selected compositions in glassy Ge_xSe_{1-x} .

moment (standard deviation) can be computed as a function of an arbitrary angle number, ranging from 1 to $N(N-1)/2$ (see labeling in the bottom panel of Fig. 2). In the forthcoming, we chose an arbitrary $N = 6$ leading to 15 different distributions and corresponding standard deviations.

IV. RIGIDITY TRANSITION

A. Angular motion

It is of interest to apply the above rationale to the Ge_xSe_{1-x} family of systems since both the elastic nature (flexible, rigid) and the connectivity are strongly dependent on composition. Figure 3 shows the standard deviations σ_{Se} and σ_{Ge} for the five Ge_xSe_{1-x} compositions as a function of the angle number (see labeling in the bottom panel of Fig. 2). Among these 15 different standard deviations, we observe that six of them display a low value for σ_{Ge} of about 10° , and four times smaller than all the others. These six σ_{Ge} 's are those associated with angular bending inside a $GeSe_{4/2}$ tetrahedron. Since only five of them are independent (the sixth angle around Ge can be determined from the knowledge of the five other angles), we conclude that such a method allows to recover exactly what is expected from a direct Maxwell constraint count³⁰ for which $n_c^{BB} = 2r_{Ge} - 3 = 5$. Similarly, one finds a single constraint (i.e., one low standard deviation, see Fig. 3(b)) for the Se atoms. A more detailed inspection shows that there is a clear difference between compositions having the six standard deviations σ_{Ge} (1,2,3,6,7,10) nearly equal ($x = 0.10$, $x = 0.20$, $x = 0.25$) and compositions belonging to the stressed rigid phase ($x = 0.33$, $x = 0.40$) which have different σ_{Ge} .

By increasing the Ge concentration the angular excursion inside the tetrahedra is seen indeed to increase [e.g., σ_{Ge} moving up to 20° for $GeSe_2$, from less than 10° in the $n = 3$ (104) PBAD] while leaving the stiffest angle (102) constant. This underscores the fact that the presence of stress will lead

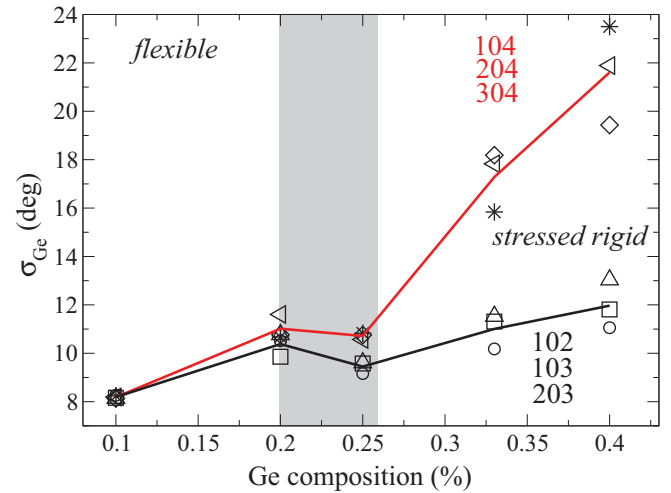


FIG. 4. (Color online) Standard deviations σ_{Ge} as a function of Ge composition, split into a contribution involving the fourth neighbor (red line, average of 104, 204, and 304) and the other contributions (black line, average of 102, 103, and 104). The shaded area corresponds to the Boolchand intermediate phase.^{16,18}

to asymmetric intratetrahedral bending motions. When the six relevant standard deviations σ_{Ge} are plotted as a function of the Ge composition (Fig. 4), the angular motion involving the fourth neighbor (PBADs 104, 204, 304) exhibits a substantial increase once the system is in the stressed rigid phase, while the others (102, 103, 203) are left with a nearly similar angular excursion. The quantity σ_{Ge} appears therefore to be an indicator of stressed rigidity.

Bending around the Se atoms is nearly unchanged with increasing Ge content, and it does not display any noticeable change when the system becomes rigid. To find a structural parameter pertaining to the Se atoms and sensitive to changes in composition, we have to resort to the dihedral angle $\bar{\delta}$ around a Se atom (see definition in Fig. 5). As shown in Table I, the dihedral angular excursion takes a value of $\sigma_{\delta} = 27.4^\circ$ for the flexible $GeSe_9$ composition and decreases significantly (down to 20° – 21°) for the compositions of rigid systems $GeSe_3$ and $GeSe_2$. Therefore, the network adapts to the predominant presence of Se atoms both by decreasing the angular variability inside the $GeSe_{4/2}$ tetrahedra, and by allowing for enhanced twisting along the Se chains.

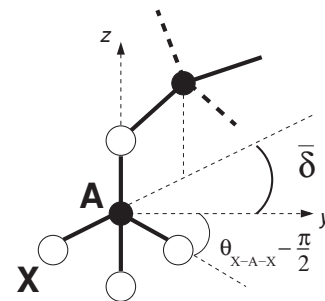


FIG. 5. Definition of the dihedral angle $\bar{\delta}$ used in the text. Note that the upper black-filled atom can be X ($r_X = 2$) or A ($r_A = 4$).

TABLE I. Mean dihedral angle $\bar{\delta}$ and standard deviation σ_{δ} of the dihedral angle distribution for seven investigated systems.

System	SiO ₂	GeO ₂	SiSe ₂	GeSe ₉	GeSe ₄	GeSe ₃	GeSe ₂
$\bar{\delta}$ (deg.)	30.9	30.4	30.9	35.0	40.3	31.9	30.6
σ_{δ} (deg.)	17.7	17.5	23.9	27.4	25.9	20.6	21.6

B. Chemical bonding

In the quest of correlations between composition changes within the Ge_xSe_{1-x} family of disordered systems and their physical properties we turn our attention to the nature of chemical bonding. As a tentative statement, one could assume that the most ionic Ge_xSe_{1-x} networks are those with the largest ratio between the amount of GeSe_{4/2} tetrahedra and the number of Ge atoms (i.e., GeSe₂). On the opposite side of the composition range, departures from stoichiometry are characterized, for $x < 0.33$, by the existence of Se chains, while for $x > 0.33$ the network has to accommodate those Ge atoms excluded from full GeSe_{4/2} tetrahedral bonding in miscoordinated units and homopolar Ge-Ge bonds.⁷ By focusing on the pair distribution function $g_{GeW}(r)$ and $g_{SeW}(r)$ we can gather information on the correlation between the localized orbitals and the distances separating the localization center from the atomic sites. Any detectable trend of these correlations with composition provides insight into the character of bonding and its variation within the Ge_xSe_{1-x} family of disordered systems.

In Figs. 6 and 7 we show the pair distribution functions $g_{GeW}(r)$ and $g_{SeW}(r)$, respectively. The interpretation of $g_{GeW}(r)$ and $g_{SeW}(r)$ is substantiated by the analysis of Fig. 8, where the positions of the Wannier centers are shown in representative subunits of Ge_xSe_{1-x} networks. Two main features common to all compositions can be seen in Fig. 6. The first is located in the vicinity of ~ 1.35 Å a distance larger than half the typical Ge-Se bond length 2.35 Å (Fig. 1). This value can be rationalized by invoking the larger electronegativity of Se atoms and the resulting electron charge transfer occurring toward the Se atoms upon formation of the GeSe₄ tetrahedron. Close observation of the maxima of the distribution in the range

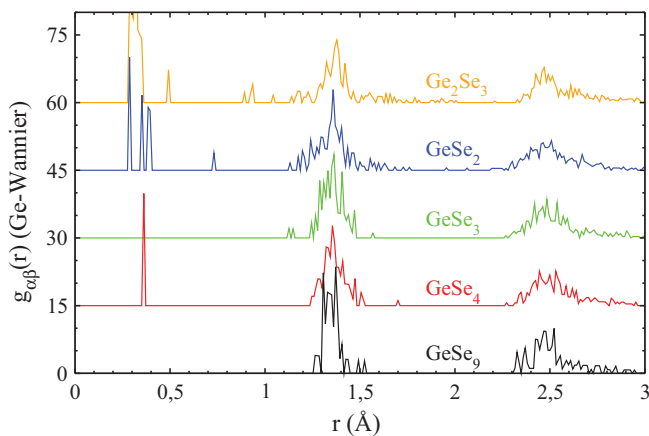


FIG. 6. (Color online) Pair distribution function $g_{GeW}(r)$ expressing the correlation between the Ge atomic sites and the position of the Wannier centers in the glassy Ge_xSe_{1-x} systems.

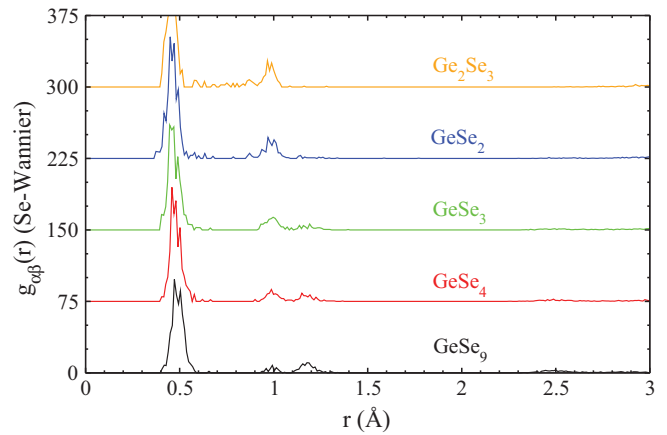


FIG. 7. (Color online) Pair distribution function $g_{SeW}(r)$ expressing the correlation between the Se atomic sites and the position of the Wannier centers in the glassy Ge_xSe_{1-x} systems.

1.35–1.5 Å reveals that the main peak slightly moves at larger values of r with an increasing concentration of Ge atoms. This indicates that the ionic character of bonding inside the GeSe₄ tetrahedron undergoes a moderate increase for growing Ge

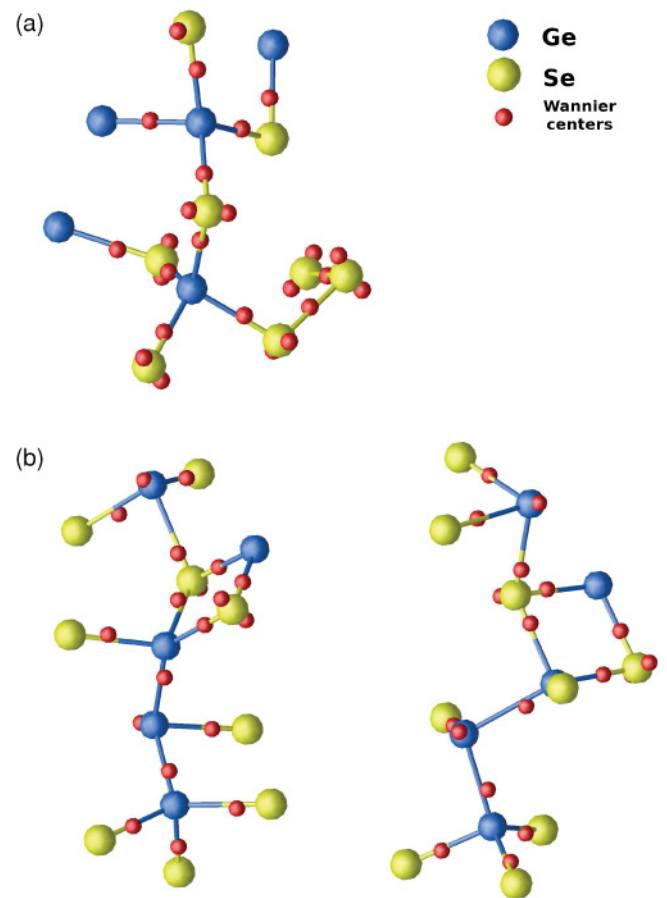


FIG. 8. (Color online) Representative subsets of Ge, Se, and Wannier centers extracted from the configurations of glassy Ge_xSe_{1-x} systems. Ge atoms appear in blue, Se atoms in yellow, and Wannier centers in red. If a bond AB exists between an atom A and an atom B, the bond is colored as follow: A→AB/2 using the color of atom A, AB/2→B using the color of atom B.

composition. Interestingly, this trend is analogous to the one followed by the dihedral angular excursion, which decreases for increasing values of x . It appears that smaller standard deviations of the dihedral angle occur in correspondence to a larger ionic character, in a way qualitatively consistent with the higher repulsion between ionic centers bearing predominant charge distribution of the same sign.

The second broad feature visible in Fig. 6 in between 2.3 and 2.5 Å can be associated to correlations between the Ge atomic sites and the Wannier centers resulting from the nonbonding Se electrons located close to the Se sites. These are easily observable in Fig. 8 when focusing on Ge-Se bonds, as they appear close to the Se atoms and, conversely, farther apart from the Ge atoms. At very short distances (smaller than 0.5 Å in the case of GeSe₄ and scattered around 0.5 Å for GeSe₂ and Ge₂Se₃) a set of sharp peaks appear in Fig. 6. These peaks are due to nonbonding electrons lying close to those Ge atoms being involved in undercoordinated, defective GeSe_{*n*} units. Examples are given in Fig. 8(b). For all compositions, Fig. 7 is characterized by a sharp peak at 0.5 Å. This peak is due to the nonbonding electrons localized around the Se site. The similar intensity of this peak for all compositions is due to the fact that these localized electrons do not depend on the number of Se atoms involved in tetrahedra and can be encountered also in the vicinity of Se atoms forming Se-made chains. A second peak of lower intensity is seen to develop at ~ 1 Å the largest intensity being reached for Ge₂Se₃. This feature can be correlated to Ge-Se bonds within the tetrahedra, its position being much smaller than half the typical Ge-Se bond length 2.35 Å (Fig. 1). In analogy with the analysis developed for the case of Ge, this value stems from the larger electronegativity of Se atoms, the centers of the localized orbitals being closer to Se atoms than to Ge atoms.

Finally, the increase in the number of Se chains with decreasing x yields the appearance of an additional bump that becomes clearly visible at 1.2 Å in GeSe₄ and GeSe₉. This bump is an indication of covalent Se-Se bonds that begin to affect the position of the Wannier centers for compositions lower than GeSe₃, this feature being absent for the latter.

V. GESE₂ UNDER PRESSURE

We apply the same analysis performed on the angular motion of Ge_{*x*}Se_{1-*x*} on a densified GeSe₂ glass. It is found that the number of neighbours around the Ge atom is still four. The neighbor (NDF) peak positions of the first four neighbors lie within the range 2.3–2.5 Å, clearly separated from the fifth neighbor peak position found at 3.25 Å. In this respect, the results on the densified system are very close to those obtained for the ambient GeSe₂ (inset of Fig. 1). Similar results are found for the Se atoms, with a gap in peak position found between $n = 1$ and $n = 2$ ($r = 2.25$ Å), and $n = 3$ ($r = 3.1$ Å). Integration of the Ge-centered and Se-centered pair distribution functions $g_{\text{Ge}}(r)$ and $g_{\text{Se}}(r)$ are in agreement with the latter analysis, and lead to $n_{\text{Ge}} = 4.1$ and $n_{\text{Se}} = 2.04$.

Figure 9 shows the 15 Ge-centered and Se-centered different PBADs. First, we remark that the angular environment around the Ge atom is nearly identical as compared to the ambient GeSe₂, with the relevant distributions still centered at the tetrahedral angle of 109°. On the other hand, we find that

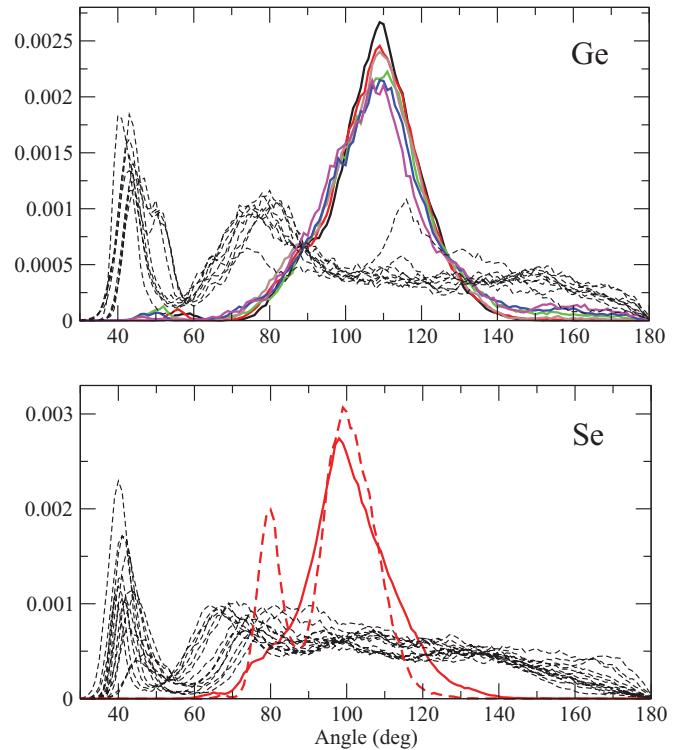


FIG. 9. (Color online) Partial bond angle distributions around Ge (top) and Se (bottom) for densified GeSe₂. The curves in color (six in the Ge PBAD and one in the Se PBAD) correspond to distributions with a low standard deviation. The broken red curve in the bottom panel serves for comparison and represents the 102 distribution of the ambient GeSe₂ glass (same as Fig. 2).

the effect of pressure has substantially modified the bimodal Se-centered bond angle distribution. In fact, the peak obtained at 80° has almost vanished to become a shoulder of the main peak at 100° that corresponds to corner-sharing tetrahedral connections. This indicates that the fraction of edge-sharing tetrahedra has been significantly reduced, consistently with results from neutron diffraction.⁵⁴ The latter show that in the pressure range 0–5 GPa, the network topology is deeply modified, the number of edge-sharing connections being severely reduced.

The corresponding standard deviations σ_{Ge} and σ_{Se} are shown in Fig. 10. While we find that the Se based standard deviation is weakly sensitive to additional stress arising from the applied pressure, we obtain an enhanced asymmetric angular motion for the Ge tetrahedra under pressure. We remind that the stressed rigid GeSe₂ displays six nonequivalent standard deviation σ_{Ge} , which contrasts with the symmetric motion found for flexible and intermediate compositions in Ge_{*x*}Se_{1-*x*}. The results obtained in densified GeSe₂ suggest that the pressure increases even more the difference between the six standard deviations. Clearly, the latter represents a measure of the presence of stress which can be driven either by composition or by densification under applied pressure.

VI. OXIDES AND CHALCOGENIDES COMPARED

We finally turn to a comparison between stoichiometric AX₂ glasses. In Fig. 2, PBADs have been shown for oxygen

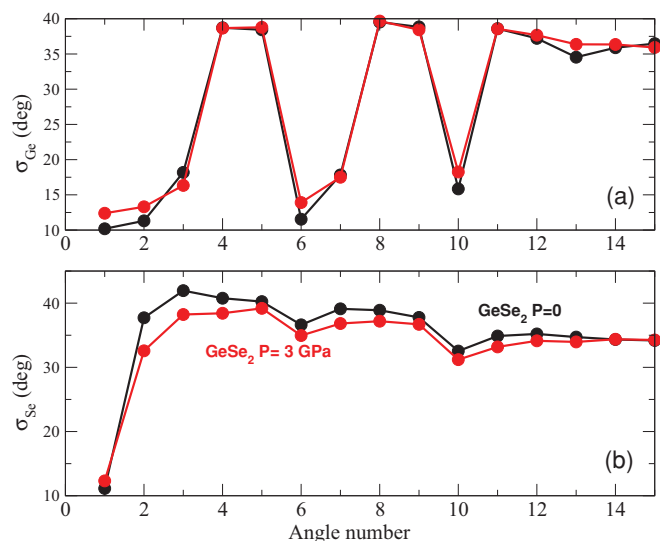


FIG. 10. (Color online) Standard deviation σ_{Ge} and σ_{Se} extracted from the partial bond angle distributions (PBAD, Fig. 9) in GeSe_2 (black line), and densified GeSe_2 (red).

(Ge-O-Ge angle) and germanium (O-Ge-O) in GeO_2 and for selenium (Ge-Se-Ge) in GeSe_2 . While oxygen displays for the principal contribution 102 (angle number 1, in red) a broad distribution centered around the angle $\theta = 135^\circ$, corresponding to the one defined by the two closest (Ge) neighbors of oxygen, secondary distributions 103 and 203 show peaks centered at around $\theta \simeq 90^\circ$ and 75° . Such a distribution contrasts with the one found for GeSe_2 which exhibits a much sharper distribution for the same 102 contribution, implying reduced angular excursions as compared to GeO_2 . Six germanium centered angles (bottom panel) are found to have almost the same distribution in GeO_2 , centered at an angle of 109° typical of the tetrahedral environment.

The behavior of the standard deviations for the PBADs is shown in Fig. 11. For all chalcogenide or oxide systems, the PBADs relative to the Group IV (Si, Ge) atom have a low standard deviation σ_{θ} , of the order of $10\text{--}20^\circ$, for instance $\sigma_{\text{Ge}} \simeq 7^\circ$ for the PBAD 102 of GeO_2 . These values are much smaller than those of the other distributions (105, 106, etc.), found close at $\simeq 40^\circ$. In addition to very low angular excursions around the tetrahedral angle of 109° (Fig. 11 top), oxides feature all σ_{θ} nearly equal for the six relevant (Ge, Si) distributions. A different situation occurs in the stoichiometric chalcogenides (Fig. 11 bottom, red curve), which exhibit increased bending for the angles defining the tetrahedra (angle 3: 104° , angle 7: 204° , etc., as already described). These results exemplify the difference in the bending nature of the tetrahedra in these two families of networks, pointing to a higher rigidity of the tetrahedra in oxides, as all angular excursions are maintained at the same low value (typically 7°).

Angle distributions around the Group VI atoms are markedly different. Indeed, the selenium standard deviation σ_{Se} of the PBAD 102 is found to be low (11.7° for GeSe_2) compared to the corresponding oxide system (26.7° for GeO_2). Therefore, the restoring effect associated with bending is much lower in GeO_2 , allowing for the identification of a *broken* angular constraint. It is worth pointing out that the standard

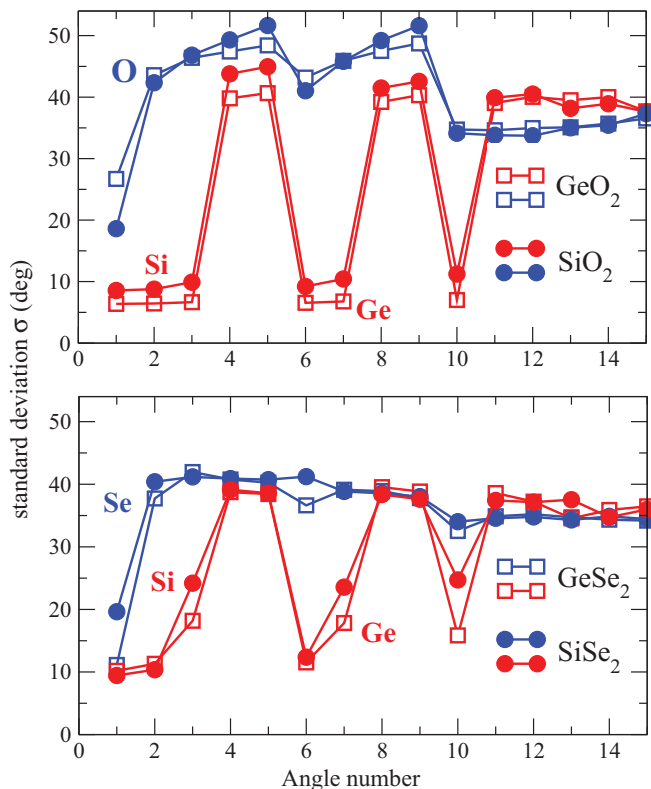


FIG. 11. (Color online) Standard deviation $\sigma_{\theta_{ij}}$ of partial bond angle distributions (PBADs) in oxides (SiO_2 , GeO_2 , top panel) and chalcogenides (SiSe_2 , GeSe_2 , bottom panel) as a function of the angle number (see definition in Fig. 2).

deviations found around 20° are close to those found in high temperature liquids ($18\text{--}25^\circ$ at 1373 K for GeSe_2), where angular constraints are assumed to be broken.^{27,55} By considering such a bending constraint as broken, the number density of constraints is reduced to $n_c = 0.33(\frac{5}{2}r_A - 3) + 0.67(\frac{5}{2}r_X - 4) = 3.00$ (i.e., oxides are optimally constrained). This result is correlated with the fact that germania (or silica) have a Ge (or Si) tetrahedral angular motion which is very similar to the one found at flexible and intermediate compositions of the $\text{Ge}_x\text{Se}_{1-x}$ system (i.e., six equivalent σ_{Ge}), also indicative of the absence of stress, as discussed above. Because of its large fraction of edge-sharing tetrahedra,³⁵ the situation of SiSe_2 appears to be somewhat intermediate with $\sigma_{\theta_{12}} = 19.6^\circ$, resulting from contributions arising from both edge-sharing and corner-sharing tetrahedra which have ineffective⁵⁶ and intact Se bond-bending constraints, respectively. The presence of six nonequivalent standard deviations in SiSe_2 indicates that this compound is stressed rigid, similarly to GeSe_2 . Experimentally, it has been found⁵⁶ that SiSe_2 belongs to the stressed rigid phase.

VII. SUMMARY AND CONCLUSION

We have shown that structural information gathered from molecular dynamics is able to provide an atomic-scale counterpart to phenomenological constraint counting concepts applied to network glasses. It appears that in such systems, most of the changes are found in angular motion, leaving the tetrahedral

character (i.e., the coordination numbers and thus the number of bond-stretching constraints) of the network unchanged under increase of stress.

In systems undergoing a rigidity transition such as $\text{Ge}_x\text{Se}_{1-x}$, it is found that the angles defining the $\text{GeSe}_{4/2}$ tetrahedron soften with decreasing Ge weight to accommodate stress, while the Se angular bending is almost unchanged. Flexibility along the Se chains is best accounted for in terms of twisting along the Se chains, found to increase with Se content. The increase of stress (or Ge content) results in an asymmetric bending motion inside the tetrahedra which appears once the system is in the stressed rigid phase, and is even enhanced if pressure is applied on the system. An analysis from Wannier functions shows that a moderate increase of the ionic character inside the GeSe_4 tetrahedron is found with growing Ge content in the $\text{Ge}_x\text{Se}_{1-x}$ system, which can be correlated with the decrease of the angular excursion of the dihedral angle.

When oxide and chalcogenide stoichiometric compositions are compared, the results show increased bending around the oxygen atom. This is consistent with a direct Maxwell constraint counting and the stress-free nature of these glasses,

which also manifests itself by an equivalent bending motion inside the Ge or Si tetrahedra, a situation also found in flexible and intermediate glasses. We obtain a clear picture of the topological differences between systems having the same composition but different chemical nature and systems made of the same species but differing in composition. The differences between glasses (oxides and chalcogenides) of same stoichiometry are rationalized in terms of amplitude of the intertetrahedral and intratetrahedral bending angular variations.

The present approach finally provides a general framework to substantiate bonding constraints theory concepts via atomic-scale simulations.

ACKNOWLEDGMENTS

It is a pleasure to acknowledge ongoing discussions with Christophe Bichara, Punit Boolchand, and Jean-Yves Raty. This work has been supported by Agence Nationale de la Recherche (ANR) No. 09-BLAN-0190-01. The calculations were performed at the IDRIS computer center of CNRS and at the Computer Center DSI of UPMC (France).

-
- ¹*Insulating and Semiconducting Glasses*, edited by P. Boolchand (World Scientific, Singapore, 2001).
- ²M. Wilson and P. S. Salmon, *Phys. Rev. Lett.* **103**, 157801 (2009).
- ³P. S. Salmon, *Proc. R. Soc. London A* **445**, 351 (1994).
- ⁴*Rigidity Theory and Applications*, edited by M. F. Thorpe and P. M. Duxbury (Kluwer Academic, New York, 1999).
- ⁵M. Micoulaut and M. Popescu, *Rigidity and Boolchand Intermediate Phases in Nanomaterials* (INOE Publishing, Bucharest, 2009).
- ⁶R. Azoulay, H. Thibierge, and A. Brenac, *J. Non-Cryst. Solids* **18**, 33 (1975).
- ⁷P. Boolchand and W. J. Bresser, *Philos. Mag.* **80**, 1757 (2000).
- ⁸D. G. Georgiev, P. Boolchand, H. Eckert, M. Micoulaut, and K. A. Jackson, *Europhys. Lett.* **62**, 49 (2003).
- ⁹C. Y. Fang, H. Yinnon, and D. R. Uhlmann, *J. Non-Cryst. Solids* **57**, 465 (1983).
- ¹⁰M. Micoulaut, *Phys. Rev. B* **74**, 184208 (2006).
- ¹¹M. Micoulaut, *Am. Mineral.* **93**, 1732 (2008).
- ¹²M. F. Thorpe and E. J. Garboczi, *Phys. Rev. B* **42**, 8405 (1990).
- ¹³R. W. Wang, M. F. Thorpe, and N. Mousseau, *Phys. Rev. B* **52**, 17191 (1995).
- ¹⁴M. T. M. Shatnawi, C. L. Farrow, P. Chen, P. Boolchand, A. Sartbaeva, M. F. Thorpe, and S. J. L. Billinge, *Phys. Rev. B* **77**, 094134 (2008).
- ¹⁵E. Bychkov, C. J. Benmore, and D. L. Price, *Phys. Rev. B* **72**, 172107 (2005).
- ¹⁶P. Boolchand, X. Feng, and W. J. Bresser, *J. Non-Cryst. Solids* **293**, 248 (2001).
- ¹⁷M. C. Weinberg, D. R. Uhlmann, and E. D. Zanotto, *J. Am. Ceram. Soc.* **72**, 2054 (1989).
- ¹⁸M. Micoulaut and J. C. Phillips, *Phys. Rev. B* **67**, 104204 (2003).
- ¹⁹M. Micoulaut and J. C. Phillips, *J. Non-Cryst. Solids* **353**, 1732 (2007).
- ²⁰K. Trachenko, M. T. Dove, V. Brazhkin, and F. S. El'kin, *Phys. Rev. Lett.* **93**, 135502 (2004).
- ²¹M. Wyart, *Ann. Phys. (Paris)* **30**, 1 (2005).
- ²²M. Zhang and P. Boolchand, *Science* **266**, 1355 (1994).
- ²³I. Farnan, P. J. Grandinetti, J. H. Baltisberger, J. F. Stebbins, U. Werner, M. A. Eastman, and A. Pines, *Nature (London)* **358**, 31 (1992).
- ²⁴M. G. Tucker, D. A. Keen, M. T. Dove, and K. Trachenko, *J. Phys. Condens. Matter* **17**, S67 (2005).
- ²⁵R. L. Mozzi and B. E. Warren, *J. Appl. Crystallogr.* **2**, 164 (1969).
- ²⁶M. Micoulaut, J.-Y. Raty, C. Otjacques, and C. Bichara, *Phys. Rev. B* **81**, 174206 (2010).
- ²⁷M. Bauchy and M. Micoulaut, *J. Non-Cryst. Solids* **357**, 2530 (2011).
- ²⁸D. A. Baker, M. A. Paesler, G. Lucovsky, S. C. Agarwal, and P. C. Taylor, *Phys. Rev. Lett.* **96**, 255501 (2006).
- ²⁹P. Richet and B. O. Mysen, *Silicate Glasses and Melts: Properties and Structure* (Elsevier, Amsterdam, 2005).
- ³⁰J. C. Phillips, *J. Non-Cryst. Solids* **34**, 153 (1979); M. F. Thorpe, *ibid.* **57**, 355 (1983).
- ³¹M. Micoulaut, Y. Guissani, and B. Guillot, *Phys. Rev. E* **73**, 031504 (2006).
- ³²B. Guillot and Y. Guissani, *J. Chem. Phys.* **104**, 7633 (1996).
- ³³C. Massobrio, A. Pasquarello, and R. Car, *J. Am. Chem. Soc.* **121**, 2943 (1999).
- ³⁴C. Massobrio, M. Micoulaut, and P. S. Salmon, *Solid State Sci.* **12**, 199 (2010).
- ³⁵M. Celino and C. Massobrio, *Phys. Rev. Lett.* **90**, 125502 (2003).
- ³⁶C. Massobrio, A. Pasquarello, and R. Car, *Phys. Rev. B* **64**, 144205 (2001).
- ³⁷C. Massobrio and A. Pasquarello, *Phys. Rev. B* **75**, 014206 (2007).
- ³⁸C. Massobrio and A. Pasquarello, *Phys. Rev. B* **77**, 144207 (2008).
- ³⁹C. Massobrio and A. Pasquarello, *J. Chem. Phys.* **114**, 7976 (2001).
- ⁴⁰L. Giacomazzi, C. Massobrio, and A. Pasquarello, *Phys. Rev. B* **75**, 174207 (2007).

- ⁴¹C. Massobrio, M. Celino, P. S. Salmon, R. A. Martin, M. Micoulaut, and A. Pasquarello, *Phys. Rev. B* **79**, 174201 (2009).
- ⁴²M. Kibalchenko, J. R. Yates, C. Massobrio, and A. Pasquarello, *Phys. Rev. B* **82**, 020202 (2010).
- ⁴³M. Cobb and D. A. Drabold, *Phys. Rev. B* **56**, 3054 (1997).
- ⁴⁴M. Cobb, D. A. Drabold, and R. L. Cappelletti, *Phys. Rev. B* **54**, 12162 (1996).
- ⁴⁵M. Durandurdu and D. A. Drabold, *Phys. Rev. B* **65**, 104208 (2002).
- ⁴⁶D. N. Tafen and D. A. Drabold, *Phys. Rev. B* **68**, 165208 (2003).
- ⁴⁷D. N. Tafen and D. A. Drabold, *Phys. Rev. B* **71**, 054206 (2005).
- ⁴⁸S. F. Boys, *Quantum Theory of Atoms, Molecules and the Solid State*, edited by P. O. Löwdin (Academic Press, New York, 1966), p. 253.
- ⁴⁹G. H. Wannier, *Phys. Rev.* **52**, 191 (1937).
- ⁵⁰N. Marzari and D. Vanderbilt, *Phys. Rev. B* **56**, 12847 (1997).
- ⁵¹R. W. Johnson, *J. Non-Cryst. Solids* **88**, 386 (1986).
- ⁵²P. S. Salmon, A. C. Barnes, R. A. Martin, and G. J. Cuello, *J. Phys. Condens. Matter* **19**, 415110 (2007).
- ⁵³R. Hussein, R. Dupree, and D. Holland, *J. Non-Cryst. Solids* **246**, 159 (1999).
- ⁵⁴P. S. Salmon, *J. Non-Cryst. Solids* **353**, 2959 (2007).
- ⁵⁵P. K. Gupta and J. C. Mauro, *J. Chem. Phys.* **130**, 094503 (2009).
- ⁵⁶D. Selvanathan, W. J. Bresser, and P. Boolchand, *Phys. Rev. B* **61**, 15061 (2000).